J. Plasma Phys. (2019), *vol.* 85, 175850101
doi:10.1017/S0022377819000102

LETTER

Wave modes in a cold pair plasma: the complete phase and group diagram point of view

Rony Keppens[1,2,†] **and Hans Goedbloed**[3]

[1]Yunnan University, Kunming, PR China

[2]Centre for mathematical Plasma Astrophysics, KU Leuven, Belgium

[3]DIFFER, TU/e Science Park, 5612AJ Eindhoven, The Netherlands

(Received 22 November 2018; revised 17 January 2019; accepted 17 January 2019)

We present a complete analysis of all wave modes in a cold pair plasma, significantly extending standard textbook treatments. Instead of identifying the maximal number of two propagating waves at fixed frequency ω, we introduce a unique labelling of all 5 mode pairs described by the general dispersion relation $\omega(k)$, starting from their natural ordering at small wavenumber k. There, the 5 pairs start off as Alfvén (A), fast magnetosonic (F), modified electrostatic (M) and electromagnetic O and X branches, and each $\omega(k)$ branch smoothly connects to large wavenumber resonances or limits. For cold pair plasmas, these 5 branches show avoided crossings, which become true crossings at exactly parallel or perpendicular orientation. Only for those orientations, we find a changed connectivity between small and large wavenumber behaviour. Analysing phase and group diagrams for all 5 wave modes, distinctly different from the Clemmow–Mullaly–Allis representation, reveals the true anisotropy of the A, M and O branches.

Key words: astrophysical plasmas, complex plasmas, plasma waves

1. Motivation

Since the advent of controlled laboratory experiments on electron–positron plasmas (Sarri *et al.* 2015), dispersion relations for waves in a pair plasma have become a diagnostic tool. Pair plasmas are created in pulsar magnetospheres or in the various flavours of ultrarelativistic astrophysical jets. Pair plasmas are also heavily studied using kinetic particle-in-cell codes, for e.g. reconnection aspects (Zenitani 2018), shocks (Bret & Narayan 2018) and turbulence (Loureiro & Boldyrev 2018). The inherent symmetry in pair plasmas leaves three length scales of interest: the cyclotron radius R_e (if magnetized), the plasma skin depth $\delta = c/\omega_p$, where c is lightspeed and ω_p is the combined electron–positron plasma frequency, and the Debye length λ_D. Laboratory pair plasmas may not necessarily achieve system sizes exceeding these wavelengths (Stenson *et al.* 2017), although most theory starts from

† Email address for correspondence: rony.keppens@kuleuven.be

spatially uniform conditions. Standard (Stix 1992; Bittencourt 2004) and modern (Thorne & Blandford 2017) textbooks describe the two-fluid viewpoint on a uniform, cold electron–ion plasma, to introduce the more complete kinetic viewpoint. Cold implies a vanishing $\lambda_D = 0$, and vanishing gyroradii when these are quantified through thermal speeds, to arrive at a zero plasma beta: we ignore all thermal pressure effects. The cold and two-fluid electron–ion assumptions imply that at fixed frequency ω, we have at most two waves that can propagate, and these are categorized as fast or slow, as right (R) or left (L) polarized, or of ordinary (O) or extraordinary (X) type. The latter two wave label pairs (R/L and O/X) relate to properties at $\vartheta = 0$ or $\vartheta = \pi/2$, respectively, where ϑ denotes the angle between the uniform magnetic field $\boldsymbol{B}$ and the wavevector $\boldsymbol{k}$ (or unit vector $\hat{\boldsymbol{n}} = \boldsymbol{k}/k$ with wavenumber k). For such cold plasmas, the Clemmow–Mullaly–Allis or CMA diagrams (Clemmow & Mullaly 1955; Stix 1992; Thorne & Blandford 2017) display the large variety in wave normal surfaces, plotting dimensionless phase velocities ω/kc versus ϑ, when varying all relevant plasma parameters. In a cold two-fluid plasma, parameter space divides into 16 different regions, where either no, a single or a pair of topologically distinct wave normal surfaces can be expected. For a cold pair plasma, this CMA diagram simplifies considerably, leaving only 5 regions to consider, as the mass symmetry makes various limiting lines coincident. These limiting lines in the CMA viewpoint on cold, two-fluid plasmas correspond to special values, like 0 or ∞, attained by the remaining dielectric tensor components. Another simplification in the cold pair plasma case is that the R and L labels become obsolete, as they both become

$$R = L = \frac{\bar{\omega}^2 - 1 - E^2}{\bar{\omega}^2 - E^2}, \tag{1.1}$$

where we introduced the dimensionless $\bar{\omega} = \omega/\omega_p$ and $E = \Omega_e/\omega_p$, with $\Omega_e = eB/m_e$ the (positively defined) cyclotron frequency of interest. Despite these simplifications, the variety of wave modes in a cold pair plasma remains intricate, with O, X and Alfvén mode types as basic ingredients, together with their resonant ($k \to \infty$) or cutoff ($k \to 0$) behaviour. Waves in equal-mass plasmas were discussed in Stewart & Laing (1992), Iwamoto (1993) and Zank & Greaves (1995), for cold and warm conditions, but our approach will reveal new aspects of cold pair plasma wave couplings and anisotropy. Pair plasmas have also been investigated in strongly magnetized ($E \gg 1$) conditions for pulsar magnetospheres (Lyutikov 1999), extending cold to warm regimes, including kinetic effects, using the usual approach based on dielectric tensor components. Extensions to account for different species bulk velocities and thermal effects are discussed in Lyutikov (1998), where the kinetic treatment reveals the mode susceptibility to e.g. two-stream cyclotron or firehose instabilities. One may even include vacuum polarization effects, and obtain a dispersion relation with coupled X and O branches due to current densities along $\boldsymbol{B}$ and finite charge densities, as in Arons & Barnard (1986). In our idealized two-fluid view, the X and O branches decouple, and all kinetic wave damping effects are ignored.

2. Cold pair plasma dispersion relation

Instead of using the dielectric tensor to obtain the dispersion relation, which has the advantage of retaining a three-by-three tensorial description when going to multiple ion–electron mixtures, the ideal two-fluid dispersion relation can also be derived from direct linearization of the equations of mass conservation, motion and energy

conservation per species, combined with the full set of Maxwell equations (Goedbloed & Poedts 2004). This leads to 14 degrees of freedom (both time-independent Maxwell equations reduce the original 16 by two), such that 14 wave modes are expected for any general (warm or cold) electron–ion mixture. Two of these modes are trivial and at marginal frequency, and this $\bar{\omega}^2 = 0$ pair relates to the single fluid magnetohydrodynamic (MHD) entropy wave. The remaining 12 can, by a judicious choice of variables, be obtained from the determinant of a symmetric 6×6 matrix, where six pairs remain in a dispersion relation of sixth order in $\bar{\omega}^2$ (Goedbloed & Poedts 2004). The symmetry of the matrix ensures that this is true at every real wavenumber k. For the specific case of a cold pair plasma, this dispersion relation further factors out a trivial $\bar{\omega}^2 = 0$ pair: the slow magnetosonic MHD waves, which become marginal at zero temperature. This results in the 5 fundamental wave pairs discussed below.

Defining $\bar{k} = \delta k$, the dispersion relation becomes a quadratic in $\bar{k}^2$ with three cubic polynomials in $\bar{\omega}^2$, but we will now systematically drop the overbars on $\bar{\omega}$ and $\bar{k}$. The final 5 pairs then derive from

$$k^4 A(\omega^2, \lambda^2) - k^2\omega^2 B(\omega^2, \lambda^2) + \omega^4 C(\omega^2) = 0, \tag{2.1}$$

where $\lambda^2 = \cos^2\vartheta$, and three third-order polynomials in ω^2 given by

$$A = (\omega^2 - E^2)(\omega^4 - \omega^2(1+E^2) + \lambda^2 E^2), \tag{2.2}$$

$$B = 2\omega^6 - 4(1+E^2)\omega^4 + [2(1+E^2)^2 + (1+\lambda^2)E^2]\omega^2 - E^2(1+E^2)(1+\lambda^2), \tag{2.3}$$

$$C = (\omega^2 - 1)(\omega^2 - 1 - E^2)^2. \tag{2.4}$$

We adopted a similar (but subtly different) notation as in standard, dielectric tensor-based treatments (Stix 1992), which opt to rewrite (2.1) to a quadratic expression in the squared refractive index $n^2 = k^2/\omega^2$. Expressions (2.2) and (2.4) instantly reveal the three cutoff limits at $k \to 0$, as $C = 0$ for $\omega^2 = 1$ (the plasma frequency) or $\omega^2 = 1 + E^2$ (twice). It also allows the resonance limits, computed from $A = 0$, to be identified as $\omega^2 = E^2$, and the pair of solutions

$$\omega_\pm^2 = \tfrac{1}{2}[1 + E^2 \pm \sqrt{(1+E^2)^2 - 4\lambda^2 E^2}]. \tag{2.5}$$

Note that ω_-^2 decreases from its parallel value $\min[1, E^2]$, to become 0 at perpendicular orientation. At the same time, ω_+^2 takes on values between $\max[1, E^2]$ for parallel propagation, and increases to $1 + E^2$ for perpendicular ($\lambda = 0$).

Identification of the 5 branches at given wavenumber k is aided as we factor (2.1) into

$$\omega^4 - \omega^2(1 + E^2 + k^2) + k^2 E^2 = 0, \tag{2.6}$$

which is the X-branch, usually written as $n^2 = R$ (this branch has wave electric field vector perpendicular to $\boldsymbol{B}$ and $\boldsymbol{k}$, and represents transverse waves, see Stewart & Laing 1992), and the O-branch in

$$\lambda^2 E^2 k^2 + \omega^2 k^2(\omega^2 - 1 - E^2) - \omega^2(\omega^2 - 1)(\omega^2 - 1 - E^2) = 0. \tag{2.7}$$

The polarization angles for the three O-branch solutions are more intricate, with varying angle between electric field and $\boldsymbol{k}$, see e.g. figure 7 in Stewart & Laing (1992). Thus far, our equations (2.6)–(2.7) are rewritten expressions, e.g. found in Lyutikov (1999) (his equation (4.1), or in the extended preprint physics/9807022,

his equations (11)–(12)), or in Stewart & Laing (1992) (their equation (15)) where they appear in terms of n^2. Their advantage is that they readily display the limits of purely parallel $\lambda = 1$ or perpendicular $\lambda = 0$ propagation, where the five branches are easily factored. Actually, (2.6)–(2.7) can be factored for arbitrary λ, using Cardano's formulae for the latter branch, but we will only need their combined expressions.

In conclusion of this section, note that the factorization of the full dispersion (2.1) into the sub-systems (2.6) and (2.7) is a fundamental one. As expanded in the following section, equation (2.6) describes the combined extraordinary electromagnetic (X) and fast magnetosonic (F) modes, whereas (2.7) describes the combined ordinary electromagnetic (O), modified electrostatic (M) and Alfvén (A) modes.

3. All waves in pair plasmas

3.1. *Group speed expressions*

Novel insight is obtained when we analyse the dispersion diagrams $\omega(k)$ for a given parameter E, and use it to quantify the group speed expressions, valid for all wavenumbers and angles ϑ. From the X-branch in (2.6), we find two angle-independent solutions

$$\omega^2_{\rm X,F} = \tfrac{1}{2}[1 + E^2 + k^2 \pm \sqrt{(1 + E^2 + k^2)^2 - 4k^2E^2}], \tag{3.1}$$

where the plus sign yields the electromagnetic X branch connecting the cutoff $1 + E^2$ to light waves as $\lim_{k\to\infty} \omega^2 = k^2$. The other angle-independent X-branch, which we label as $\omega_{\rm F}$, has a minus sign before the square root in (3.1), and is directly linked to the fast MHD modes, since $\lim_{k\to 0} \omega^2/k^2 = E^2/(1 + E^2)$. At (cyclotron) resonance, this branch has $\lim_{k\to\infty} \omega^2 = E^2$. For both branches, it is easy to quantify the phase speed and group speed for every value of k, and the latter are

$$\frac{\partial \omega}{\partial \boldsymbol{k}}_{|\rm X,F} = \frac{k\hat{\boldsymbol{n}}}{2\omega}\left[1 \pm \frac{1 - E^2 + k^2}{\sqrt{(1 + E^2 + k^2)^2 - 4k^2E^2}}\right], \tag{3.2}$$

with the plus sign for the electromagnetic X branch $\omega_{\rm X}(k)$, and the minus sign for the fast branch $\omega_{\rm F}(k)$. This is an isotropic circle (sphere) at all wavenumbers, and the $\omega_{\rm F}$ one has vanishing radius $\propto 1/k^3$ as $k \to \infty$, while at small wavenumbers, it retrieves the fast part $\pm E\hat{\boldsymbol{n}}/\sqrt{1 + E^2}$ of the well-known MHD Friedrichs diagram showing the group speed for all angles ϑ. The $\omega_{\rm X}$ mode also has a circular group diagram, with radius $k/(1 + E^2)^{3/2}$ at large wavelengths, while tending to the light circle $\partial\omega/\partial\boldsymbol{k} \to \pm\hat{\boldsymbol{n}}$ at large k, appropriate for light waves.

We can use (2.7) to deduce the governing group speed expression on all three other branches, which we will label as $\omega_{\rm O,M,A}$, written in a manner that aids direct evaluation for limits towards small and large wavenumbers. We use implicit derivation to $\partial/\partial\boldsymbol{k}$, noting that $\partial k^2/\partial\boldsymbol{k} = 2\boldsymbol{k}$ and $\partial\lambda^2/\partial\boldsymbol{k} = 2\lambda/k[\hat{\boldsymbol{b}} - \lambda\hat{\boldsymbol{n}}]$ where $\hat{\boldsymbol{b}} = \boldsymbol{B}/B$, and write their group speed as

$$\frac{\partial \omega}{\partial \boldsymbol{k}}_{|\rm O,M,A} = \frac{\lambda k E^2[\hat{\boldsymbol{b}} - \lambda\hat{\boldsymbol{n}}] + k\hat{\boldsymbol{n}}(\omega^2 - \omega^2_+)(\omega^2 - \omega^2_-)}{\omega[1 + E^2 - 2\omega^2(2 + E^2) + 3\omega^4 + k^2(1 + E^2 - 2\omega^2)]}. \tag{3.3}$$

This general expression can be used to derive all small and large wavenumber limits. To do so, we note that (2.7) can be rewritten in terms of refractive index as $n^2 = (\omega^2 - 1)(\omega^2 - 1 - E^2)/[\lambda^2E^2 + \omega^2(\omega^2 - 1 - E^2)]$. From this expression, low frequency

limits render us the Alfvén branch where $\omega^2 = \lambda^2 k^2 E^2/(1+E^2)$, while high frequency behaviour becomes electromagnetic, or $\omega^2 \propto k^2$. More precisely, the same expression can be shown to give $\lim_{k\to\infty} \omega^2 = 1 + k^2$, for the electromagnetic O-branch.

We now analyse (3.3) in all relevant limits, and find for the behaviour as $k \to 0$ while Alfvénic, the familiar

$$\frac{\partial \omega}{\partial \boldsymbol{k}}_{|_{\mathrm{A},k\to 0}} = \mathrm{sgn}(\lambda)\frac{E}{\sqrt{1+E^2}}\hat{\boldsymbol{b}}, \tag{3.4}$$

which is the purely point-like group speed of Alfvén waves, also part of the MHD Friedrichs diagram. Anticipating that this $\omega_{\mathrm{A}}(k,\vartheta)$ branch will transform to resonant behaviour and will normally connect to ω_- (see next section), we find at resonance

$$\frac{\partial \omega}{\partial \boldsymbol{k}}_{|_{\mathrm{A},k\to\infty}} = \frac{\lambda E^2[\hat{\boldsymbol{b}} - \lambda\hat{\boldsymbol{n}}]}{k(\omega_+^2 - \omega_-^2)\omega_-}. \tag{3.5}$$

At the branch to the ω_+ resonance, which will be labelled as $\omega_{\mathrm{M}}(k,\vartheta)$ as this will modify the electrostatic cutoff $\omega_{\mathrm{M}}(k\to 0) = 1$, we find a similar expression, namely

$$\frac{\partial \omega}{\partial \boldsymbol{k}}_{|_{\mathrm{M},k\to\infty}} = \frac{-\lambda E^2[\hat{\boldsymbol{b}} - \lambda\hat{\boldsymbol{n}}]}{k(\omega_+^2 - \omega_-^2)\omega_+}. \tag{3.6}$$

The behaviour for the electromagnetic O-branch going as $\omega^2 = 1 + k^2$ is to leading order the expected $\partial\omega/\partial\boldsymbol{k} \to \pm\hat{\boldsymbol{n}}$ at large k. At the remaining two cutoffs, we find extreme anisotropic behaviour. For $\omega_{\mathrm{M}}(k\to 0)$ at the plasma frequency cutoff, we find

$$\frac{\partial \omega}{\partial \boldsymbol{k}}_{|_{\omega\to 1,k\to 0}} = \pm k(0, \sin\vartheta), \tag{3.7}$$

where we used the freedom to take $\hat{\boldsymbol{b}} = (1, 0)$ and $\hat{\boldsymbol{n}} = (\cos\vartheta, \sin\vartheta)$. Equation (3.7) represents energy transport purely perpendicular to the magnetic field, in the $\boldsymbol{k} - \boldsymbol{B}$ plane. Finally, for the other cutoff at $1 + E^2$ which defines the start of the remaining $\omega_{\mathrm{O}}(k,\vartheta)$ branch, we get

$$\frac{\partial \omega}{\partial \boldsymbol{k}}_{|_{\omega^2\to 1+E^2,k\to 0}} = \frac{\pm k}{(1+E^2)^{3/2}}(\cos\vartheta, 0). \tag{3.8}$$

Equation (3.8) represents energy transport purely along the magnetic field. We will show later the visual confirmation of all these limits, at both small and large wavelengths, but the actual variation implied by (3.3) is extremely intricate, especially near $k \approx O(1)$. We first turn attention to a judicious labelling of branches.

3.2. *Avoided crossings of branches*

In this section, we discuss the complete dispersion $\omega(k)$ diagrams for varying $\vartheta \in [0, \pi/2]$. At $\lambda = 1$ or parallel propagation $\vartheta = 0$, the 3 branches mixed up in (2.7) are an ω_{A} Alfvénic branch that overlaps with the fast ω_{F} one (hence $\omega_{\mathrm{A}}(k, \vartheta = 0)$ has the same cyclotron resonant behaviour), an electromagnetic ω_{O} one that is identical to ω_{X} from (3.1) and the electrostatic $\omega^2 = 1$ mode pair. It does seem that only 3 modes are left, but two are doubly degenerate. Also for this parallel case, when $E > 1$, the coincident ω_{A} and ω_{F} branches obviously intersect the electrostatic branch, and

this happens at $\omega^2 = 1$, $k^2 = E^2/(E^2 - 1)$. This intersection was already noted, albeit in approximate form for $E \gg 1$ only, in Lyutikov (1999) (preprint version, equation (15)). At exactly perpendicular propagation, a similarly complete factorization of all 5 wave modes is easily achieved, since now for $\lambda = 0$ the Alfvénic branch becomes marginal $\omega_A^2 = 0$ and the two branches remaining in (2.7) become $\omega^2 = 1 + k^2$ and $\omega^2 = 1 + E^2$. Clearly, the latter two branches also intersect, and this for the values $\omega^2 = 1 + E^2$, $k^2 = E^2$. Hence, the extreme cases of pure parallel or pure perpendicular propagation are exactly known, and those are typically used to start the subsequent categorization of plasma wave modes. However, both cases are rather exceptional, as we demonstrate now.

Indeed, drawing and analysing the dispersion diagrams for all angles $0 < \vartheta < \pi/2$, it is noted that the ordering of all 5 branches is unaltered for all wavenumbers k, and is such that $\omega_A < \omega_F < \omega_M < \omega_O < \omega_X$, where we labelled the branches as Alfvénic, fast, modified electrostatic and both O and X electromagnetic types. At all angles except 0 or $\pi/2$, branches do not cross, and can be best ordered according to the way in which their robust small wavenumber behaviour (and their associated group speed appearance) connects to the large wavenumber behaviour. In figure 1, we show dispersion diagrams for 4 representative angles for a case with $E = 1.5$. This E-value is chosen to show both avoided crossings mentioned (only one appears when $E \leqslant 1$), and represents a case where one can not rely on approximations using $E \gg 1$. The second diagram of figure 1 (taken at $\vartheta = \pi/3$) shows clearly how (i) the angle-dependent $\omega_A(k, \vartheta)$ branch connects the Alfvén group diagram at small k to the ω_- resonance, and (ii) the angle-independent $\omega_F(k)$ branch lies above ω_A in frequency, and connects the fast circular group speed at small k to the cyclotron $\omega = E$ resonance. Above ω_F lies the modified electrostatic branch which we indicated with $\omega_M(k, \vartheta)$, which connects the lowest cutoff $\omega = 1$ with the highest resonance ω_+. The remaining $\omega_{O,X}$ branches both start at the (coincident) cutoff where $\omega = \sqrt{1 + E^2}$, and go off to their light speed behaviour at small wavelength (large k). The fact that this happens for all $0 < \vartheta < \pi/2$ should be appreciated as avoided crossings of branches, which is illustrated in figure 1 by drawing the dispersion relation also for two extremely small deviations from parallel (i.e. $\vartheta = \epsilon$) or perpendicular (i.e. $\vartheta = \pi/2 - \epsilon$) orientation, where we took $\epsilon = 0.002$ for illustration purposes. The avoided crossings are only clear when zooming in on the regions of interest, i.e. at the values $(\sqrt{1 + E^2}, E)$ (for near perpendicular) and $(1, \sqrt{E^2/(E^2 - 1)})$ (near parallel), and these are shown as figure insets. The latter, near-parallel behaviour is also discussed in Lyutikov (1999), but this particular avoided crossing is obviously only relevant for cases where $E > 1$. In that sense, the avoided crossing between the ω_M (purple branch in figure 1) and the ω_O branch (cyan in the figure) at near-perpendicular propagation, is more robust, as it occurs at all values of $E > 0$.

The near-parallel avoided crossing becomes a true crossing of branches at exactly parallel propagation, as then the $\omega_A(k, 0)$ branch suddenly connects to the ω_+ resonance, which coincides with the cyclotron resonance E at this angle. The near-perpendicular avoided crossing becomes a true crossing at exactly perpendicular propagation, when this time the $\omega_M(k, \pi/2)$ (purple) branch connects to light waves, while the (cyan) ω_O branch becomes of constant frequency $\sqrt{1 + E^2}$, which is the ω_+ resonance for this angle. These avoided crossings are related to the observation that the original dispersion relation is only quadratic in k^2, such that at fixed real frequency (i.e. at every horizontal intersection through our dispersion diagrams), at most two wave modes can be found. This observation is at the basis of the CMA diagrams, and is embedded in all theory regarding cold two-fluid plasma waves,

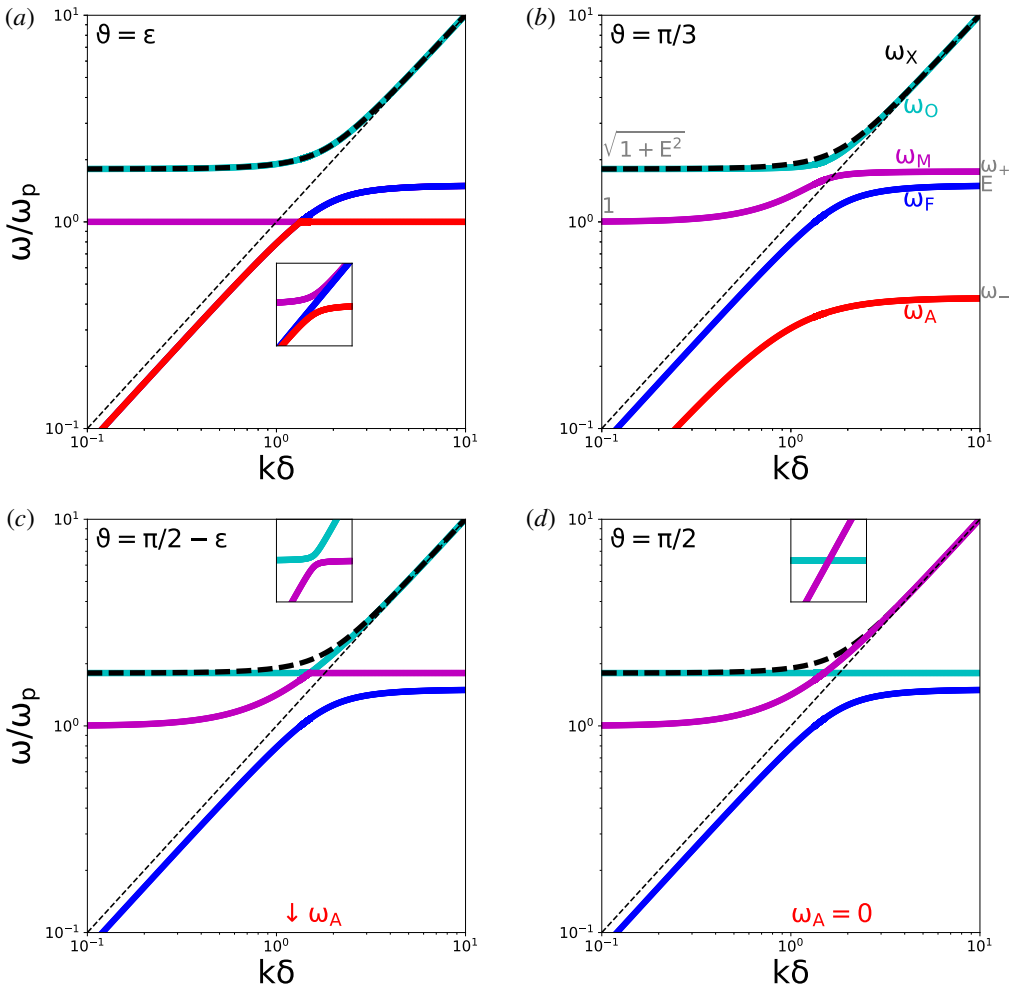

FIGURE 1. The dispersion diagram showing all 5 $\omega(k)$ branches for a pair plasma with $E = 1.5$. Panels (*a–d*) differ in angle ϑ between wavevector and magnetic field. An animation of the variation with ϑ is given in the supplementary material, in the movie DispersionRelation.mp4 available at https://doi.org/10.1017/S0022377819000102. The thin dashed line indicates light speed behaviour. Insets for near-parallel or perpendicular angles ϑ illustrate avoided crossings. Branches are coloured black (angle-independent $\omega_X(k)$), blue (angle-independent $\omega_F(k)$), cyan ($\omega_O(k, \vartheta)$), purple ($\omega_M(k, \vartheta)$) and red ($\omega_A(k, \vartheta)$). The ω_X branch uses dashes, to better distinguish it from the ω_O branch which nearly overlaps.

which labels wave types as fast or slow, L/R or X/O at fixed frequency. However, this accepted naming convention is confusing, since our fast ω_F branch then changes label from fast when $\omega_F < 1$, to slow for $1 < \omega_F < E$, for the case displayed in figure 1. Moreover, the cold assumption got rid of the MHD slow mode, which enriches the classification when a warm plasma is considered. Finally, even the extraordinary (X) versus ordinary (O) mode label seems misleading, as the X-branch is not showing any special behaviour: both its modes (ω_F and ω_X) are angle independent and do not show any coupling to other branches, in contrast to all 3 mode pairs $\omega_{A,M,O}$ from the O-branch family.

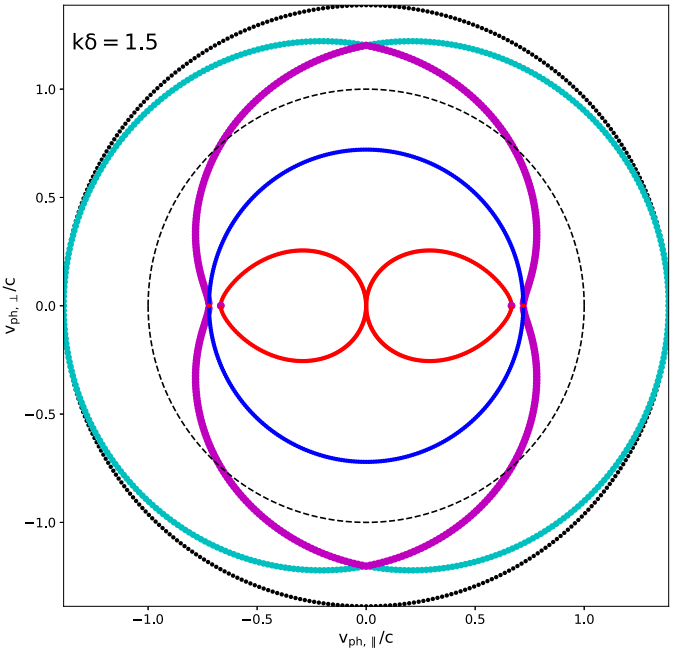

FIGURE 2. A representative phase diagram of all 5 wave modes for all angles, at fixed wavenumber $\bar{k} = 1.5$. The strict ordering of wave frequencies for all angles $0 < \vartheta < \pi/2$ ensures these diagrams to be nested. At the chosen wavenumber, the modified electrostatic $\omega_{\rm M}$ (purple) and the electromagnetic O branch $\omega_{\rm O}$ (cyan) coincide at perpendicular orientation, and for larger k they will have exchanged labels for this orientation. Such an exchange already occurred for parallel orientation between the red ($\omega_{\rm A}$) and purple ($\omega_{\rm M}$) branch. The dashed circle indicates the light speed. An animation of this variation with wavenumber is provided as supplementary material in the movie Phasediagram.mp4.

3.3. *Phase and group speed diagrams*

We now present the complete phase and group speed diagrams, collecting all information of the various wave types for all angles and wavenumbers. Figure 2 shows a representative phase diagram for the case $E = 1.5$, earlier shown in dispersion diagram view in figure 1. Animating this diagram for varying wavenumber k shows clearly how the branch exchange witnessed at exactly parallel or perpendicular orientation occurs when the phase diagrams of two wave modes suddenly coincide at specific k-values. The diagram shown is for a k value that exactly demonstrates this coincidence of branches at perpendicular orientation (along the central vertical in the figure). Exchange of wave mode types at parallel orientation (along the central horizontal in the figure) already switched an $\omega_{\rm A}$ with an $\omega_{\rm M}$ mode (hence the purple dots on the red branch, and the red dots on the purple branch). It is to be noted that these phase diagrams are different from the ones usually shown as wave normal surfaces in the CMA view: we plot $[\omega/kc](\vartheta)$ for fixed k-value, accounting for all 5 wave modes, textbook treatments plot $[\omega/kc](\vartheta)$ for fixed frequency ω, and hence mix information from varying wavenumbers (as horizontal intersections at fixed ω in dispersion views of figure 1 show the k values to change with angle ϑ). The point to note is that $k(\omega, \vartheta)$, and (2.1) allows a maximal 2 modes at fixed ω, while we emphasize one has exactly 5 modes for every real k. Note that superluminal phase

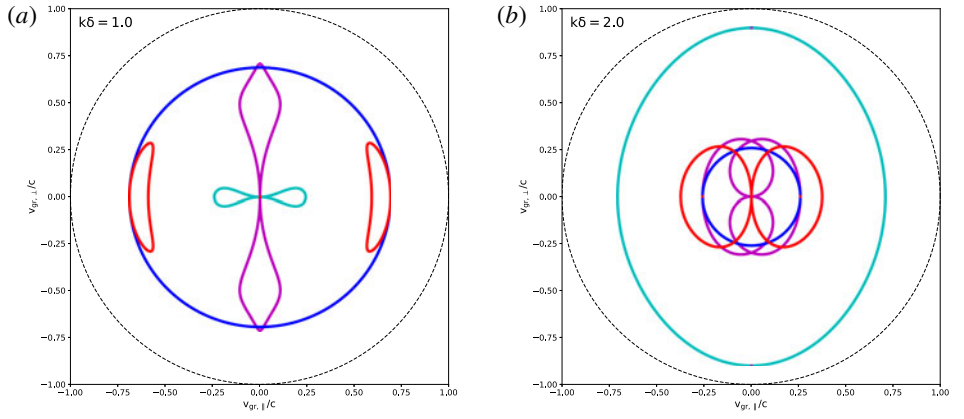

FIGURE 3. Representative group diagrams showing all 5 wave modes for all angles, at fixed wavenumbers $\bar{k} = 1$ and 2 (*a*,*b*). The dashed circle indicates light speed. An animation of this variation with $\bar{k}$ is provided as supplementary material in the movie Groupdiagram.mp4.

speeds are encountered for solutions $\omega(k)$ above the dashed lines in figure 1, or equivalently outside the dashed circle in figure 2. Animated views for figure 1 are in the movie entitled `DispersionRelation.mp4`, and for figure 2 in the movie entitled `Phasediagram.mp4`.

The group speed diagrams for all 5 wave modes can also be computed for every wavenumber k. These diagrams directly enrich the well-known Friedrich diagrams for MHD (Goedbloed & Poedts 2004), which visually display the extreme anisotropic wave behaviour of slow, Alfvén and fast modes at large wavelengths, low frequencies. In the cold pair plasma case, the slow pair is marginal, but Alfvén and fast remain, as in (3.4)–(3.2). Figure 3 shows the complete group diagram for $E = 1.5$, at $k = 1$ and $k = 2$. The true complexity of the variation with wavenumber can only be appreciated in animated views (provided as supplementary material in the movie entitle Groupdiagram.mp4), but they correspond to the formulae in (3.2)–(3.3) (with limits as in (3.4)–(3.8)). The animation shows the intricate reshaping of the group speed curves, especially near the special values where branches cross (i.e. at $k^2 = E^2$ and at $k^2 = E^2/(E^2 - 1)$ when $E > 1$). For all three wave modes ω_A, ω_M and ω_O which demonstrate coupling and exchange of mode limits at small wavelengths, the energy flow as quantified through these group diagrams is strongly anisotropic, and a proper visualization of their variation with wavenumber k requires us to pay full attention to sudden variations with angle ϑ, especially at near-parallel or near-perpendicular orientations. Note that, as physically required, all group speeds are always found within the light circle. Finally, limit cases can now be fully understood as special instances of these 5 wave mode pairs: the unmagnetized ($E = 0$) cold pair plasma leaves $\omega_M = 1$ as electrostatic modes, both electromagnetic $\omega_{O,X}$ pairs coincide on $\omega^2 = 1 + k^2$, while Alfvénic and fast branches become marginal. The strongly magnetized $E \to \infty$ case, moves the electromagnetic waves to infinite frequencies, and keeps the ω_M, ω_F and ω_A branches.

4. Conclusions

Our treatment of all wave mode pairs in a cold pair plasma provides, for the first time, a complete categorization of all wave anisotropies inherent in cold pair plasmas.

This is best appreciated from our quantification of the phase and group speed for all 5 mode pairs, at all wavenumbers and angles (i.e. our equations (3.2)–(3.3) and the animations provided with figures 2 and 3). Rather than working in terms of the breaking index n^2, our starting point was the general twelfth-order dispersion relation for warm plasmas, containing six mode pair solutions (e.g. Goedbloed & Poedts 2004), which reduce to 5 non-trivial ω^2 solutions in the cold limit. A quantification of the mode polarizations should best employ the 6 variables used there to obtain a fully symmetric matrix representation. A completely similar treatment can be done for cold electron–ion cases (where two parameters will enter, E and its counterpart for ions $I = \Omega_i/\omega_p$), or for warm plasmas (where also the thermal speeds of the species come in). Still, the polynomial form of the dispersion relation renders computing all six ω^2 pairs for warm plasmas fairly trivial, and the quantification of group speeds along all six $\omega(k, \vartheta)$ branches becomes possible. For warm plasmas, avoided crossings between several branches may show up at intermediate angles, instead of at the extremes of purely parallel or perpendicular orientations as illustrated here. The slow MHD wave will form the extra ingredient to categorize all 6 wave modes in warm plasmas, starting from their ordering in frequency as found at large wavelengths. Avoided crossings will cause more intricate reorderings of branches, as connectivity to small wavelength limits at resonances or electromagnetic limits can change with angle ϑ.

Although our discussion is based on an ideal two-fluid viewpoint, this forms the basis of more realistic kinetic treatments which all employ the dielectric tensor formulation. A useful intermediate step would be to incorporate collisional effects, such as done in Stewart & Laing (1992) or in Goedbloed & Poedts (2004). This would already allow for wave damping, and in warm plasmas, handling pressure anisotropy will open the route to firehose instabilities. Allowing for relative streaming of both species will break the symmetry of the forward–backward pairs in the fluid limit, a phenomenon known to introduce fascinating complexities to the MHD wave part of the spectrum (Goedbloed, Keppens & Poedts 2010, 2019).

Acknowledgements

This research was supported by the KU Leuven (GOA/2015-014). R.K. thanks Yunnan University and C. Xia for kind hospitality during his sabbatical stay.

Supplementary movies

Supplementary movies are available at https://doi.org/10.1017/S0022377819000102.

REFERENCES

Arons, J. & Barnard, J. J. 1986 Wave propagation in pulsar magnetospheres – dispersion relations and normal modes of plasmas in superstrong magnetic fields. *Astrophys. J.* **302**, 120–137.

Bittencourt, J. A. 2004 *Fundamentals of Plasma Physics*, 3rd edn. Springer.

Bret, A. & Narayan, R. 2018 Density jump as a function of magnetic field strength for parallel collisionless shocks in pair plasmas. *J. Plasma Phys.* **84** (6), 905840604.

Clemmow, P. C. & Mullaly, R. F. 1955 The dependence of the refractive index in magneto-ionic theory on the direction of the wave normal. In *Physics of the Ionosphere*, p. 340.

Goedbloed, J. P., Keppens, R. & Poedts, S. 2010 *Advanced Magnetohydrodynamics*. Cambridge University Press.

GOEDBLOED, J. P., KEPPENS, R. & POEDTS, S. 2019 *Magnetohydrodynamics of Laboratory and Astrophysical Plasmas*. Cambridge University Press.

GOEDBLOED, J. P. & POEDTS, S. 2004 *Principles of Magnetohydrodynamics*. Cambridge University Press.

IWAMOTO, N. 1993 Collective modes in nonrelativistic electron–positron plasmas. *Phys. Rev.* E **47**, 604–611.

LOUREIRO, N. F. & BOLDYREV, S. 2018 Turbulence in magnetized pair plasmas. *Astrophys. J. Lett.* **866**, L14.

LYUTIKOV, M. 1998 Waves in a one-dimensional magnetized relativistic pair plasma. *Mon. Not. R. Astron. Soc.* **293**, 447.

LYUTIKOV, M. 1999 Beam instabilities in a magnetized pair plasma. *J. Plasma Phys.* **62**, 65–86.

SARRI, G., PODER, K., COLE, J. M., SCHUMAKER, W., DI PIAZZA, A., REVILLE, B., DZELZAINIS, T., DORIA, D., GIZZI, L. A., GRITTANI, G. *et al.* 2015 Generation of neutral and high-density electron–positron pair plasmas in the laboratory. *Nat. Commun.* **6**, 6747.

STENSON, E. V., HORN-STANJA, J., STONEKING, M. R. & SUNN PEDERSEN, T. 2017 Debye length and plasma skin depth: two length scales of interest in the creation and diagnosis of laboratory pair plasmas. *J. Plasma Phys.* **83**, 595830106.

STEWART, G. A. & LAING, E. W. 1992 Wave propagation in equal-mass plasmas. *J. Plasma Phys.* **47**, 295–319.

STIX, T. H. 1992 *Waves in Plasmas*. American Institute of Physics.

THORNE, K. S. & BLANDFORD, R. D. 2017 *Modern Classical Physics: Optics, Fluids, Plasmas, Elasticity, Relativity, and Statistical Physics*. Princeton University Press.

ZANK, G. P. & GREAVES, R. G. 1995 Linear and nonlinear modes in nonrelativistic electron–positron plasmas. *Phys. Rev.* E **51**, 6079–6090.

ZENITANI, S. 2018 Dissipation in relativistic pair-plasma reconnection: revisited. *Plasma Phys. Control. Fusion* **60** (1), 014028.